Effect of growth time on morphology and photoelectrochemical performance of TiO_2 nanorod arrays grown on transparent conducting substrates*

SUI Mei-rong (隋美蓉)[1]**, **HAN Cui-ping** (韩翠平)[1], **GU Xiu-quan** (顾修全)[2], **WANG Yong** (王永)[1], **TANG Lu** (唐璐)[1], **and TANG Hui** (唐慧)[1]

1. School of Medical Imaging, Xuzhou Medical College, Xuzhou 221004, China

2. School of Materials Science and Engineering, China University of Mining and Technology, Xuzhou 221116, China

(Received 8 September 2015)

TiO_2 nanorod arrays (NRAs) were synthesized directly on the fluorine tin oxide (FTO) coated glass substrates by a facile hydrothermal route. The effects of growth time on the photoelectrochemical (PEC) properties of TiO_2 NRAs are investigated. The samples synthesized for 4 h exhibit a photocurrent intensity of 0.37 mA/cm^2 at the irradiation of Xe lamp and a bias of 0 V. As the growth time increases, the thickness and order degree of the NRAs are enhanced, but the photocurrent is reduced a lot. It might be associated with the hindering of a high background electron density in NRs due to the long-time hydrothermal reaction in acid environment. Moreover, the decline behavior is observed, which is attributed to the poor charge separation capacity of TiO_2 array electrodes and could be suppressed efficiently by applying a suitable positive bias.

Document code: A **Article ID:** 1673-1905(2015)06-0405-5

DOI 10.1007/s11801-015-5170-3

Up to now, TiO_2 is still one of the most important semiconductor photocatalysts which have both high stability and surface energy[1]. It is possible to synthesize the ultrathin TiO_2 nanostructures with a good dispersibility and a large specific surface area[2]. The mesoporous TiO_2 films were widely applied as the photoanodes of dye-sensitized solar cells (DSSCs), with a high conversion efficiency of 13%[3,4]. However, the large-scale application of such a material is limited by its wide band-gap (~3.2 eV), leading to a low conversion efficiency of solar energy (less than 5%). Currently, a few visible-light response semiconductor photocatalysts have been developed, such as Ag_3PO_4, $BiVO_4$, α-Fe_2O_3 and so on[5-7]. Nevertheless, those semiconductors exhibit either lower catalytic activity or poorer stability than TiO_2. Otherwise, it is an efficient way to enhance the visible-light response of TiO_2 by doping or modification with other components[8].

Recently, one-dimensional (1D) TiO_2 nanorod arrays (NRAs) grown directly on fluorine tin oxide (FTO) substrates have received much attention because they are transparent and provide a direct and rapid way to transport the carriers[9,10]. H. Wang et al[11] reported a CdS quantum dot (QD)-sensitized single-crystalline rutile TiO_2 NRA on FTO substrate used as the photoelectrodes of photoelectrochemical (PEC) solar cells and it exhibited a photocurrent intensity of ~5.8 mA/cm^2 at 0 V bias. C. Wang et al[12] from another group demonstrated the use of Fe doping treatment as a facile and effective strategy to improve the PEC water-splitting performance of TiO_2 NRAs at the visible-light irradiation. Moreover, very recently, X. Wang et al[13] synthesized a Bi_2S_3/rGO modified TiO_2 NRA structure and demonstrated an efficiency of 1.2% at 0.47 V bias at irradiation of visible light.

In this study, we report the preparation and PEC performance of hydrothermally synthesized transparent TiO_2 NRAs, and discuss the effect of growth time on the PEC activities. It is found that the samples grown for 4 h exhibit the best PEC activity.

TiO_2 NRAs were synthesized directly on FTO glass by a facile one-pot hydrothermal route, which have been widely reported previously[9,10]. Briefly, 30 mL concentrated HCl (38%) was added into 30 mL de-ion water and stirred for 2 min. Afterwards, 1 mL titanium isopropoxide was dissolved into the above solution. Then, 30 mL of the mixed solution was taken out and transferred into a Teflon-lined stainless steel autoclave (100 mL). The FTO substrates were placed into the autoclave with the conductive side facing down. Then, the hydrothermal reaction was carried out at 150 °C for a certain time. Finally, the autoclave was cooled to room temperature (RT)

* This work has been supported by the Natural Science Foundation of Xuzhou City (No.KC14SM088), and the Natural Science Foundation Project of Jiangsu Province (No.BK20130198).

** E-mail:smr2012@xzmc.edu.cn

and the FTO substrates were taken out, followed by a sintering process in a muffle furnace at 450 °C for 30 min in air to increase the crystallinity and adhesion of TiO_2 NRAs.

The prepared samples were studied by powder X-ray diffraction (XRD, D8) which was performed at 20 kV and 30 mA with Cu Ka radiation (λ=0.154 06 nm). Field-emission scanning electron microscopy (FESEM, Sirion 200) was used to identify the morphology of TiO_2 NRAs. The optical absorption spectra were investigated with a Cary 300 UV-vis diffusion spectrophotometer in wavelength range of 200–900 nm ($BaSO_4$ as a reference sample).

Linear sweep voltammetry (LSV) and photocurrent response (*I-t*) were achieved in a three-electrode cell which was connected with a potentiostat (CHI660D, CH Instruments) and at the irradiation of a 500 W Xe lamp (Beijing Trusttech). The lamp provided full-range light with an irradiation intensity of ~100 $mW \cdot cm^{-2}$. Besides, in our study, TiO_2 NRAs were used as the work electrodes, while a Pt foil and a saturated calomel electrode (SCE) were employed as the counter electrode (CE) and reference electrode, respectively. Meanwhile, a 0.5 mol/L Na_2SO_4 aqueous solution was used as the electrolyte. The electrochemical impedance spectra (EIS) were conducted using CHI660D with an alternating current signal (10 mV) in the frequency range of 0.1–10^5 Hz at open circuit potential (OCP). The Mott-Schottky (M-S) plots were measured at a frequency of 1 kHz in the dark.

Figs.1 and 2 display the XRD pattern and SEM images of TiO_2 NRAs grown on FTO substrates. As can be seen, the (101) and (002) planes from the TiO_2 rutile phase are clearly identified, while the other peaks are assigned to SnO_2 from the FTO substrate. Meanwhile, those TiO_2 NRs also exhibit the average diameter of ~150 nm, which are grown epitaxially and directly on FTO layers due to a small lattice mismatch (2%) between SnO_2 and rutile FTO crystals. The TiO_2 NRs are orientated disorderly in the samples synthesized for 2 h, while not only the NR length is increased but also the orientation gets more aligned with the increasing growth time. The 4 h sample exhibits the average length of 1.8 μm, while the value is 2.2 μm for the 6 h sample.

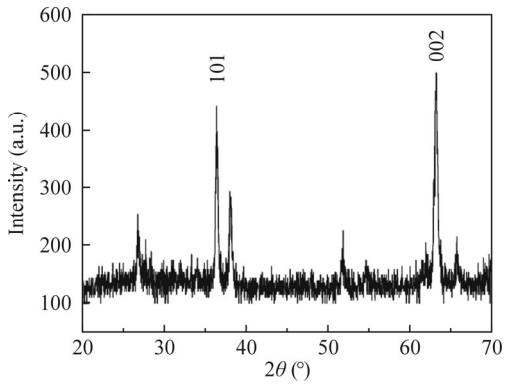

Fig.1 Typical XRD pattern of TiO_2 NRAs grown on FTO substrates at 150 °C for 4 h

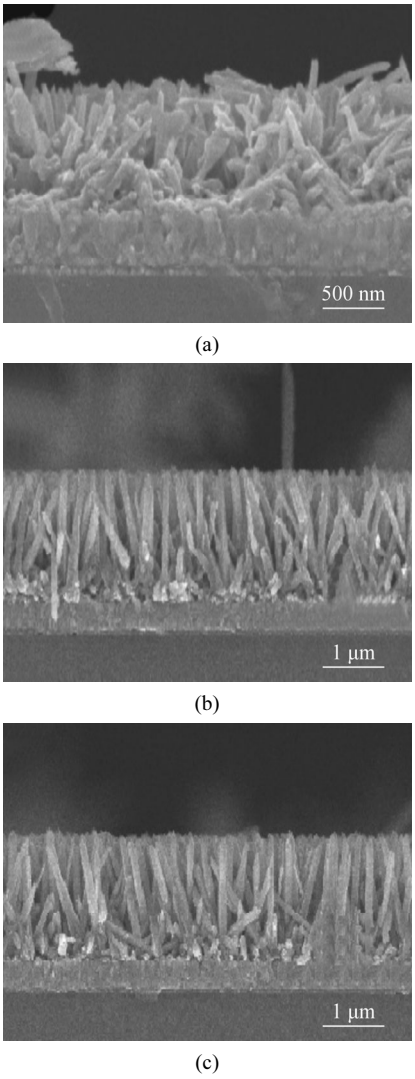

Fig.2 FESEM images of TiO_2 NRAs grown on FTO substrates at 150 °C for (a) 2 h, (b) 4 h and (c) 6 h, respectively

Fig.3 shows the UV-vis diffusion absorption of TiO_2 NRAs grown on FTO. The sharp absorption edges appear in the range of 3.0–3.2 eV, indicative of the well crystallized samples. The 2 h sample has a fundamental bandgap of 3.07 eV, which is reduced to 3.04 eV and 3.02 eV for the 4 h and 6 h synthesized samples, respectively. Totally, there is no obvious change in the bandgap value or optical absorption coefficient.

Fig.4 shows the LSV curves of TiO_2 NRAs grown on FTO layers at a full-range irradiation from a Xe lamp. The 500 W Xe lamp can provide a full range irradiation including the UV and visible light, so TiO_2 can also be excited to produce the carriers despite of the wide bandgap (~3.0 eV). As shown, the 4 h sample exhibits the highest photocurrent density, which is 0.37 mA/cm^2 at 0 V and 1.44 mA/cm^2 at 0.5 V, respectively. Meanwhile, it is worth noting that the 6 h sample exhibits the lowest photocurrent intensity although it has the largest average length of NRs.

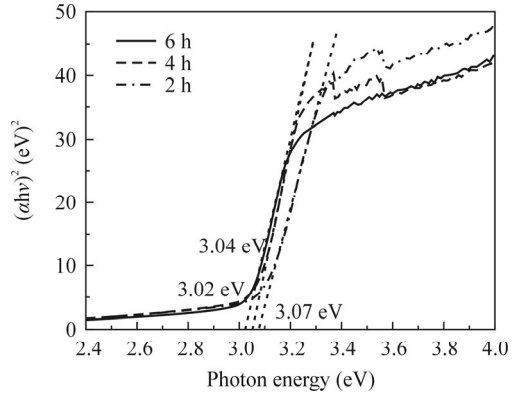

Fig.3 UV-vis diffusion absorption spectra of TiO_2 NRAs grown on FTO substrates at 150 °C for 2 h, 4 h and 6 h, respectively

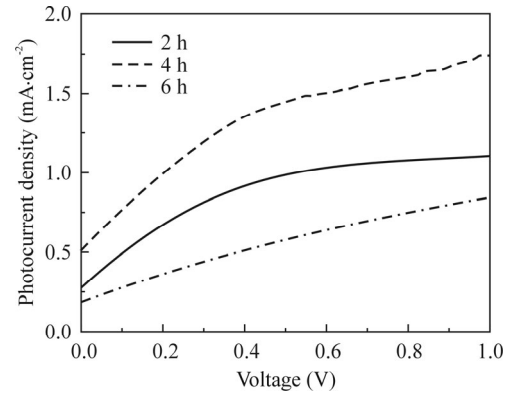

Fig.4 LSV curves of TiO_2 NRAs grown on FTO substrates at 150 °C for 2 h, 4 h and 6 h, respectively

Fig.5 shows the photoresponse (*I-t*) curves of TiO_2 NRAs at the interrupted irradiation. All the samples exhibit the high on/off ratios of the current values, suggesting that the TiO_2 NRAs have good photo-responsibility. Consistent with Fig.4, the 4 h sample displays the highest photocurrent intensity of all, while the dark current intensities from three samples are comparable. Moreover, a series of sharp peaks appear in the curves soon after the light on/off, indicative of the instability of photocurrent. In details, the photocurrent of the 4 h sample declines by ~50% during the first 30 s. That phenomenon was also observed in the $WO_3/BiVO_4$ photoanodes by Grimes et al[14], and they attributed it to the poor charge separation or high carrier recombination inside the electrodes. Specifically, when the light is turned on, the carriers accumulated at the TiO_2/electrolyte interfaces are transferred out immediately towards the external circuit, leading to a high transient photocurrent density. But the vacancies couldn't be supplemented efficiently and timely due to a limitation in the charge separation rates, resulting in a rapid decay in the photocurrent.

Theoretically, the sharp peaks in *I-t* curves could be eliminated by enhancing the charge separation of the TiO_2 NRA electrodes. In order to confirm it, the *I-t* curves of TiO_2 NRAs at various positive biases (0 V, 0.3 V and 0.6 V) are indicated in Fig.6. It is clearly observed that the sharp peaks get weaker and weaker with the increasing positive bias. Besides, the photocurrent intensity also gets enhanced significantly. In other words, enhancing the charge separation is an efficient way to obtain high and stable photocurrent intensity. The corresponding schematic model for the generation and separation process of the photoexcited carriers is given in Fig.7. At a positive bias, the high build-in electric field could ensure the enough and continual carriers can be collected by the external circuit, producing a high and stable photocurrent.

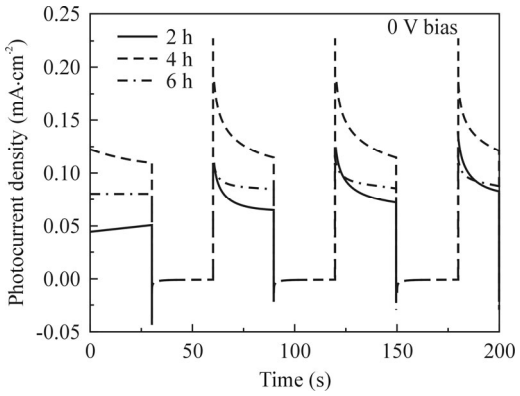

Fig.5 *I-t* curves of TiO_2 NRAs grown on FTO substrates at 150 °C for 2 h, 4 h and 6 h, respectively with a time interval of 30 s

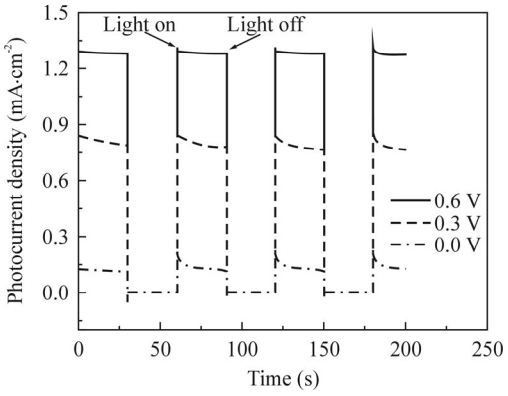

Fig.6 *I-t* curves of 4 h TiO_2 NRAs measured at various positive bias values of 0 V, 0.3 V and 0.6 V, respectively with an irradiation intensity of 100 mW/cm^2

Fig.8 shows the Nyquist plots of TiO_2 NRAs operated at OCP and an irradiation. An equivalent circuit model (b) is also provided for the curve fitting, and the corresponding results are indicated in Tab.1. The resistances of the electrodes include two parts: the series resistance (R_s) and the charge transferring (or transport) resistance (R_{ct}). Evidently, the 6 h sample exhibits a higher value of R_{ct} than other two ones, implying its low transport capacity of photo-generated carriers. It might be the main reason for the poor photocurrent indicated in Fig.4.

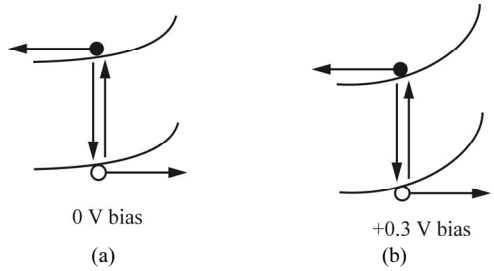

Fig.7 Schematic models for illustrating the generation and separation process of photoexcited carriers in TiO_2 electrodes: (a) At zero bias; (b) At +0.3 V bias

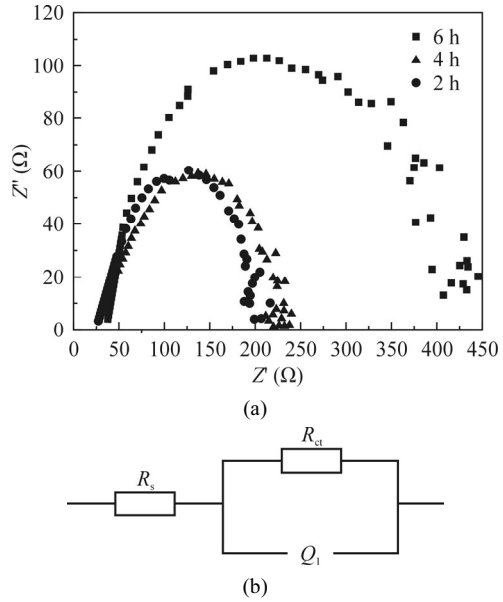

Fig.8 (a) EIS (Nyquist) plots of TiO_2 NRAs grown on FTO substrates for various times (2—6 h) at the irradiation; (b) An equivalent circuit model for fitting the Nyquist plots

Tab.1 Calculated electronic parameters from EIS spectra (Nyquist plots) with an illumination intensity of 100 mW/cm^2

Sample (growth time/h)	R_s/Ω	R_{ct}/Ω
2	27	180
4	33	201
6	34	329

Fig.9 shows the M-S plots of TiO_2 NRAs in the dark. It is a typical characteristic of n-type semiconductor, since the curve slope is positive. As is well known, the correlation between depletion layer capacitance (C) and applied potential (V) could be described by the following equation[15]:

$$\frac{1}{C^2}=\frac{2}{e_0\varepsilon\varepsilon_0 N_d}\left(V-V_{fb}-\frac{kT}{e_0}\right), \tag{2}$$

where e_0 is the electron charge, ε is the dielectric constant, ε_0 is the permittivity of vacuum, N_d is the donor density, V is the applied potential, V_{fb} is the flat-band potential, and kT/e_0 is a temperature-dependent correction term. By a fitting, the N_d and V_{fb} values are deduced and indicated in Tab.2. There is no obvious difference in the V_{fb} value for those samples, while N_d of the 6 h sample is significantly lower than those of other samples. It implies that there might be a higher background electron density in the 6 h sample than other two samples. Those background carriers might result from the defects generated during the long-time hydrothermal process. And the presence of high concentration background carriers or donor-like defects hinders the charge transport inside TiO_2 NRAs, leading to the poor photocurrent.

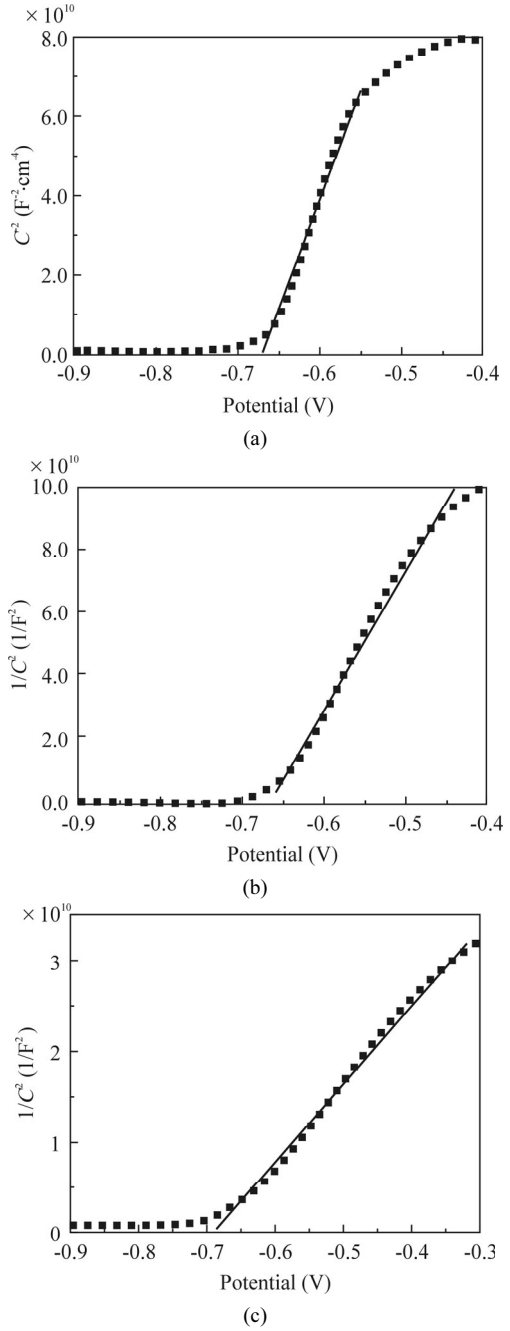

Fig.9 Mott-Schottky (M-S) plots of TiO_2 NRAs obtained in the dark grown on FTO substrates for (a) 2 h, (b) 4 h, and (c) 6 h, respectively

Tab.2 Calculated electronic parameters from Mott-Schottky plots obtained in the dark

Sample (growth time/h)	Slope/10^{11}	Flat band V_{fb}/V	Electron density $N_d/10^{16}$ cm^{-3}
2	5.48	−0.70	1.0
4	4.37	−0.70	1.3
6	0.86	−0.72	6.4

In summary, TiO_2 NRAs have been synthesized on FTO substrates directly by one-pot hydrothermal methods, followed by a sintering process at 450 °C for 30 min. Afterwards, the PEC activities of those TiO_2 NRAs are investigated. It is found that the 4 h TiO_2 NRA sample exhibits the highest photocurrent density, which is attributed to both the large surface area and the good charge transport ability. Although the 6 h grown sample might have a larger surface area, the background electron density is also increased significantly, leading to a larger hindering during the carrier transport process and a lower photocurrent intensity. In addition, it is observed that both the intensity and stability of the photocurrent could be enhanced by applying a positive bias on the work electrodes, which is attributed to the improved charge separation.

References

[1] Y. Ma, X. Wang, Y. Jia, X. Chen, H. Han and C. Li, Chem. Rev. **114**, 9987 (2014).

[2] H.B. Wu, H.H. Hng and X.W. Lou, Adv. Mater. **24**, 2567 (2012).

[3] B. O'Regan and M. Gräztel, Nature **353**, 737 (1991).

[4] S. Mathew, A. Yella, P. Gao, R. Humphry-Baker, B. F. E. Curchod, N. Ashari- Astani, I. Tavernelli, U. Rothlisberger, Md. K. Nazeeruddin and M. Grätzel, Nat. Chem. **6**, 242 (2014).

[5] H. Tong, S. Ouyang, Y. Bi, N. Umezawa, M. Oshikiri and J. Ye, Adv. Mater. **24**, 229 (2012).

[6] C. Du, X. Yang, M.T. Mayer, H. Hoyt, J. Xie, G. McMahon, G. Bischoping and D. Wang, Angew. Chem. Int. Ed. **52**, 12692 (2013).

[7] W.J. Jo, J.W. Jang, K. Kong, H.J. Kang, J.Y. Kim, H. Jun, K.P.S. Parmar and J.S. Lee, Angew. Chem. Int. Ed. **51**, 3147 (2012).

[8] Z. Zou, J. Ye, K. Sayama and H. Arakawa, Nature **414**, 625 (2001).

[9] B. Liu and E.S. Aydil, J. Am. Chem. Soc. **131**, 3985 (2009).

[10] X.Q. Gu, Y.L. Zhao and Y.H. Qiang, J. Mater. Sci. Mat. Electron. **23**, 1373 (2012).

[11] H. Wang, Y. Bai, H. Zhang, Z. Zhang, J. Li and L. Guo, J. Phys. Chem. C **114**, 16451 (2010).

[12] C. Wang, Z. Chen, H. Jin, C. Cao, J. Li and Z. Mi, J. Mater. Chem. A **2**, 17820 (2014).

[13] X. Wang, J. Xie and C. M. Li, J. Mater. Chem. A **3**, 1235 (2015).

[14] J. Su, L. Guo, N. Bao and C.A. Grimes, Nano Lett. **11**, 1928 (2011).

[15] H. P. Maruska and A. K. Ghosh, Sol. Energy **20**, 443 (1978).